Probing nuclear structure with mean transverse momentum in relativistic isobar collisions

Hao-jie Xu [1,2] Wenbin Zhao,[3] Hanlin Li,[4] Ying Zhou,[5] Lie-Wen Chen,[5] and Fuqiang Wang [1,2,6]

[1]*School of Science, Huzhou University, Huzhou, Zhejiang 313000, China*
[2]*Strong-Coupling Physics International Research Laboratory (SPiRL), Huzhou University, Huzhou, Zhejiang 313000, China*
[3]*Department of Physics and Astronomy, Wayne State University, Detroit, Michigan 48201, USA*
[4]*College of Science, Wuhan University of Science and Technology, Wuhan, Hubei 430065, China*
[5]*School of Physics and Astronomy, Shanghai Key Laboratory for Particle Physics and Cosmology, and Key Laboratory for Particle*
Astrophysics and Cosmology (MOE), Shanghai Jiao Tong University, Shanghai 200240, China
[6]*Department of Physics and Astronomy, Purdue University, West Lafayette, Indiana 47907, USA*

Transverse momentum ($p_\perp$) generation in relativistic heavy-ion collisions is sensitive to the initial geometry and the final-state bulk evolution. We demonstrate with hydrodynamic calculations that the mean $p_\perp$ ratio ($R_{\langle p_\perp \rangle}$) between the highly similar isobar $^{96}_{44}\mathrm{Ru} + ^{96}_{44}\mathrm{Ru}$ and $^{96}_{40}\mathrm{Zr} + ^{96}_{40}\mathrm{Zr}$ collisions is insensitive to the bulk evolution and remains sensitive to the small difference in the initial nuclear structure (neutron skin and deformation) between the Ru and Zr nuclei. We further find that nuclear deformation can produce an anticorrelation between $R_{\langle p_\perp \rangle}$ and eccentricity (or elliptic flow) in central collisions. These findings suggest that the $R_{\langle p_\perp \rangle}$ between the isobar systems can be used to measure the neutron skin thickness and deformation parameters, which can, in turn, constrain the nuclear symmetry energy slope parameter.

Introduction. Relativistic heavy-ion collisions at BNL's Relativistic Heavy Ion Collider (RHIC) and CERN's Large Hadron Collider (LHC) create a strongly coupled quark-gluon plasma (QGP), governed by quantum chromodynamics (QCD) [1–4]. The evolution of the QGP medium can be successfully described by relativistic hydrodynamics with a nearly minimum value of the shear viscosity to entropy density ratio η/s in nature [5–10]. The mean transverse momentum ($\langle p_\perp \rangle$) of hadrons in relativistic heavy-ion collisions reflects the expansion strength of the formed hot and dense QCD medium. With the same total entropy (energy), a denser initial condition would lead to a faster expansion and thus a larger radial flow and $\langle p_\perp \rangle$ [11–15]. This connection between initial collision geometry and final observables provides a potential opportunity to probe the structure of the colliding nuclei [16,17]. However, the magnitude of $\langle p_\perp \rangle$ itself strongly depends on the bulk properties of the medium. To describe experimental data, a finite bulk viscosity is required in hydrodynamic calculations [18,19]. Thus, in order to probe the initial geometry, one has to rely on $\langle p_\perp \rangle$ fluctuations and correlations to anisotropic flow to eliminate large uncertainties in the $\langle p_\perp \rangle$ magnitudes caused by uncertainties in the dynamic evolution [11–15].

On the other hand, one may exploit collisions of isobar nuclei where the dynamic evolution is similar—so its uncertainties cancel in their comparisons—but the initial geometries are different. The isobar collisions of $^{96}_{44}\mathrm{Ru} + ^{96}_{44}\mathrm{Ru}$ and $^{96}_{40}\mathrm{Zr} + ^{96}_{40}\mathrm{Zr}$ were originally proposed to control the background in search of the chiral magnetic effect (CME) [20–25]. Such collisions were conducted in 2018, and the STAR Collaboration has collected $\sim 2 \times 10^9$ events for each collision species [26]. Previous studies have indicated that the nuclear density distributions of the two isobar nuclei differ [27]. The nuclear structure difference can cause significant observable differences between the isobar systems, such as in their event multiplicities and elliptic flows, that are crucial to the CME search [27–29]. Indeed, those differences have been observed in isobar data [26] and are consistent with the predictions from energy density functional theory (DFT) calculations [27–29]. The DFT calculations indicate a large halo-type neutron skin thickness (Δr_{np}) for the $^{96}\mathrm{Zr}$ nucleus [30]; the Δr_{np} is 0.183 fm for $^{96}\mathrm{Zr}$ and 0.042 fm for $^{96}\mathrm{Ru}$ with a reasonable parameter set (see Ref. [30]). The neutron skin difference between $^{96}\mathrm{Zr}$ and $^{96}\mathrm{Ru}$ comes from the neutron-proton asymmetry in nuclear matter equations of state, which is encoded by the symmetry energy [31–33].

The DFT calculations are based on well-established nucleon-nucleon potential parameters in the extend Skyrme-Hartree-Fock model fitting experimental data [34,35]. The density slope parameter of the symmetry energy is fitted to be $L(\rho_c) = 47.3$ MeV at a subsaturation cross density of $\rho_c = 0.11\rho_0/0.16 \simeq 0.11$ fm^{-3} [35–37]. The DFT calculation with the same model parameters gives a neutron skin thickness of $\Delta r_{\mathrm{np}} = 0.190$ fm for the benchmark $^{208}\mathrm{Pb}$ nucleus [30]. However, the recent PREX-II measurement using parity-violating electroweak interactions has yielded a large neutron skin thickness of the $^{208}\mathrm{Pb}$ nucleus of $\Delta r_{\mathrm{np}} = 0.283 \pm 0.071$ fm [38], leading to a larger density slope parameter of $L(\rho_c) = 71.5 \pm 22.6$ MeV [39], at tension with the world data established by strong interaction means.

Owing to the large statistics of isobar collisions, the differences between the two collision systems can be measured very

precisely. We have proposed that the multiplicity difference between the isobar collisions can be used to probe the neutron skin and the symmetry energy slope parameter [30]. Some of us have suggested that the elliptic flow measurements can also determine the proper nuclear structures of the isobar nuclei [29]. In this Letter, we further show that the $\langle p_\perp \rangle$ ratio in relativistic isobar collisions,

$$R_{\langle p_\perp \rangle} = \frac{\langle p_\perp \rangle^{\text{Ru+Ru}}}{\langle p_\perp \rangle^{\text{Zr+Zr}}}, \tag{1}$$

can also be used to probe nuclear structures and that this ratio has weak dependence on transport properties of the collision system. We also study the effect of nuclear deformation on $R_{\langle p_\perp \rangle}$ and demonstrate, together with elliptic flow measurements, that both the neutron skin thickness and the deformation can be determined. This work supplements our previous work on multiplicity difference between the isobar systems in probing nuclear structures.

Model description and initial conditions. In this study, the $\langle p_\perp \rangle$ is calculated by the iEBE-VISHNU model [40–42], an event-by-event (2+1)-dimensional viscous hydrodynamics, together with the hadron cascade model [ultrarelativistic quantum molecular dynamics (UrQMD)] to simulate the evolution of the subsequent hadronic matter [43,44]. The initial condition of the collision is obtained by the Trento model [42,45], given a nuclear density distribution. After a short free streaming, the evolution of the initial energy momentum tensor in hydrodynamics follows the conservation law $\partial_\mu T^{\mu\nu} = 0$. All the parameters for the iEBE-VISHNU simulation are taken from Ref. [19] and were calibrated to experimental data at the LHC, except the normalization factor to match the multiplicity in isobar collisions at the RHIC [26].

For the initial condition, the nuclear density distribution of the colliding nuclei is incorporated into the Trento model. Similar to our previous study [29,30,46], the isobar nuclear densities are assumed to be spherical and calculated by DFT with three density slope parameters, $L(\rho_c) = 20$, 47.3, and 70 MeV. The calculated densities are parametrized [29] by the Woods-Saxon (WS) distributions

$$\rho = \frac{\rho_0}{1 + \exp{(r - R)/a}}, \tag{2}$$

$$R = R_0\big(1 + \beta_2 Y_2^0 + \beta_3 Y_3^0 + \cdots\big), \tag{3}$$

where the deformity parameters β_2 and β_3 are set to zero. The R_0 and a parameters are determined by matching the $\langle r \rangle$ and $\langle r^2 \rangle$ quantities to those from the DFT-calculated densities [29]. The ρ_0 parameter is fixed by normalization of the nucleus volume. The corresponding WS parameters are listed in Table I. Because we use the WS parametrizations instead of the DFT-calculated densities throughout this Letter, we simply denote those WS densities as Lc20, Lc47, and Lc70.

There is strong evidence from anisotropic flow (v_n) measurements in central isobar collisions that the Ru and Zr nuclei have different deformations [26]. Those measurements suggest [47] that the ^{96}Ru nucleus has a quadrupole deformation, while the ^{96}Zr nucleus has an octupole deformation. DFT calculations of deformed nuclei are challenging and usually yield large uncertainties. It is not clear how deformation

TABLE I. WS parametrizations (radius parameter R_0 and diffuseness parameter a) of the ^{96}Ru and ^{96}Zr nuclear density distributions, matching to the corresponding $\langle r \rangle$ and $\langle r^2 \rangle$ from the Lc20, Lc47, and Lc70 spherical densities calculated by DFT. The ρ_0 value is fixed by volume normalization. The WS parametrization of the ^{96}Ru (^{96}Zr) nuclear density with an assumed quadrupole (octupole) deformity parameter of $\beta_2 = 0.16$ ($\beta_3 = 0.16$), keeping the ρ_0 value and matching to the volume and the rms radius of the spherical Lc47 density, is also listed. The quoted values for R_0 and a are in fm and those for ρ_0 are in 1/fm^3.

	^{96}Ru				^{96}Zr			
	ρ_0	R	a	β_2	ρ_0	R	a	β_3
Lc20	0.161	5.076	0.483	0.00	0.166	4.994	0.528	0.00
Lc47	0.159	5.093	0.488	0.00	0.163	5.022	0.538	0.00
Lc70	0.157	5.114	0.487	0.00	0.160	5.045	0.543	0.00
Lc47Def	0.159	5.090	0.473	0.16	0.163	5.016	0.527	0.16

affects the nucleus size with respect to that of the spherical nucleus. In this study, the WS parameters R_0 and a for the given $\beta_2 = 0.16$ (or $\beta_3 = 0.16$) are calculated to match the volume and the root mean square (rms) of the corresponding nucleus calculated by DFT with $L(\rho_c) = 47.3$ MeV, keeping the normalization ρ_0 value fixed. These parameters are also listed in Table I, denoted as Lc47Def.

It is well known that the $\langle p_\perp \rangle$ is related to the transverse energy density in heavy-ion collisions [11,14], approximately by

$$\langle p_\perp \rangle \propto d_\perp \equiv \sqrt{N_{\text{part}}/S_\perp}, \tag{4}$$

where N_{part} is the number of participant nucleons and $S_\perp$ is the transverse overlap area. The neutron skin affects $S_\perp$, so the $\langle p_\perp \rangle$ is sensitive to the neutron skin thickness. Because the latter depends on $L(\rho_c)$, the $\langle p_\perp \rangle$ can be used to probe the $L(\rho_c)$ parameter. The overlap area can be calculated by [14,48]

$$S_\perp = \pi \sqrt{\langle x^2 \rangle \langle y^2 \rangle - \langle xy \rangle^2} \equiv \pi \langle r_\perp^2 \rangle \sqrt{1 - \epsilon_2^2}, \tag{5}$$

where

$$\langle r_\perp^2 \rangle \equiv \langle x^2 + y^2 \rangle \tag{6}$$

and

$$\epsilon_2^2 \equiv \frac{((\langle y^2 \rangle - \langle x^2 \rangle)^2 + 4\langle xy \rangle^2}{\langle x^2 + y^2 \rangle^2} \tag{7}$$

are the rms and the eccentricity of the overlap area, respectively. It is clear from Eq. (5) that nuclear deformation also affects $S_\perp$. In the spherical case, $r_\perp$ is affected by the neutron skin; in the deformed case, $r_\perp$ is affected by both the neutron skin and β_2.

In this study, we simulate $\sim 1.6 \times 10^6$ hydrodynamic events each for Zr + Zr and Ru + Ru collisions, together with 50 oversamplings of UrQMD afterburner for each hydrodynamic event. With such statistics, we are able to determine the $R_{\langle p_\perp \rangle}$ to the precision of 10^{-5} in a given centrality; therefore, the statistical errors are not visible for the results presented in this Letter. Even considering potential underestimation of the statistical uncertainties from the UrQMD oversampling, the
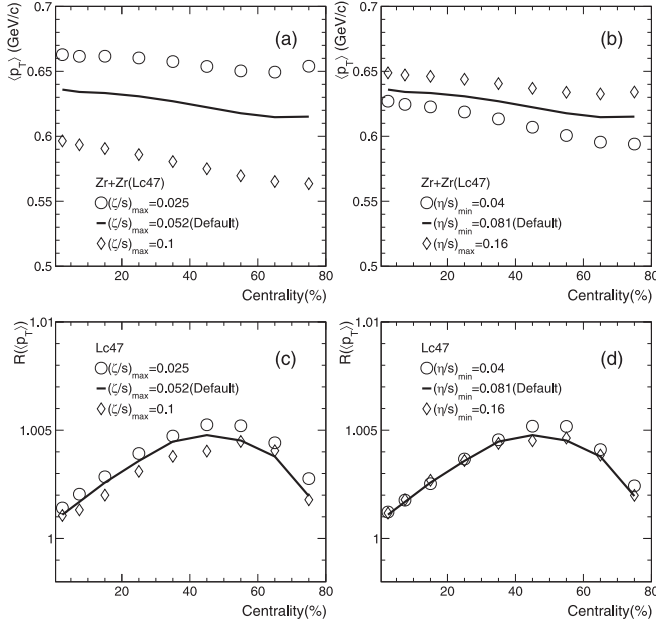
FIG. 1. [(a), (b)] The mean transverse momentum $\langle p_\perp \rangle$ as functions of centrality in $Zr + Zr$ collisions, calculated by the iEBE-VISHNU model with different $(\eta/s)_{\min} = 0.04$, 0.08, and 0.12 and $(\zeta/s)_{\max} = 0.025$, 0.052, and 0.1 with WS parametrization to the Lc47 spherical densities. [(c), (d)] The corresponding $Ru + Ru/Zr + Zr$ ratio $R_{\langle p_\perp \rangle}$.

precision is still well under control, especially for the most central collisions. We note that the $R_{\langle p_\perp \rangle}$ can be measured even more precisely in experiment, where $\sim 2 \times 10^9$ good events have been collected for each isobar collision system [26].

Results. In hydrodynamics, the $\langle p_\perp \rangle$ values are sensitive to the medium bulk properties. To investigate the effects of bulk properties, we calculate the $\langle p_\perp \rangle$ values using the Lc47 densities with three values of shear viscosity [$(\eta/s)_{\min} = 0.04$, 0.08, and 0.16] and with three values of bulk viscosity [$(\zeta/s)_{\max} = 0.025$, 0.081, and 0.1], respectively. The middle values are typical values used in hydrodynamic simulations [19]. The results are depicted in Figs. 1(a) and 1(b), which show strong sensitivities of $\langle p_\perp \rangle$ to those bulk properties, especially to the bulk viscosity, consistent with previous studies [18]. Those bulk properties, however, have little effect on the centrality-dependent ratio $R_{\langle p_\perp \rangle}$ between $Ru + Ru$ and $Zr + Zr$ collisions, as shown in Figs. 1(c) and 1(d). The largest variation in the ratio $R_{\langle p_\perp \rangle}$ from the relatively large ranges of the medium viscosity is on the order of 0.001. This finding strongly indicates that, while the magnitude of $\langle p_\perp \rangle$ depends on the bulk properties, the ratio $R_{\langle p_\perp \rangle}$ is insensitive to them and, hence, their uncertainties.

Having demonstrated the insensitivity of $R_{\langle p_\perp \rangle}$ to the bulk properties, we now investigate effects of the initial condition of nuclear density. Figure 2(a) presents the $\langle p_\perp \rangle$ as functions of centrality in both $Ru + Ru$ and $Zr + Zr$ collisions from the iEBE-VISHNU simulations with various DFT-calculated spherical densities for the isobars. Larger $L(\rho_c)$ gives thicker neutron skin and larger $S_\perp$, and results in smaller $\langle p_\perp \rangle$ at each centrality, as expected. On the other hand, the
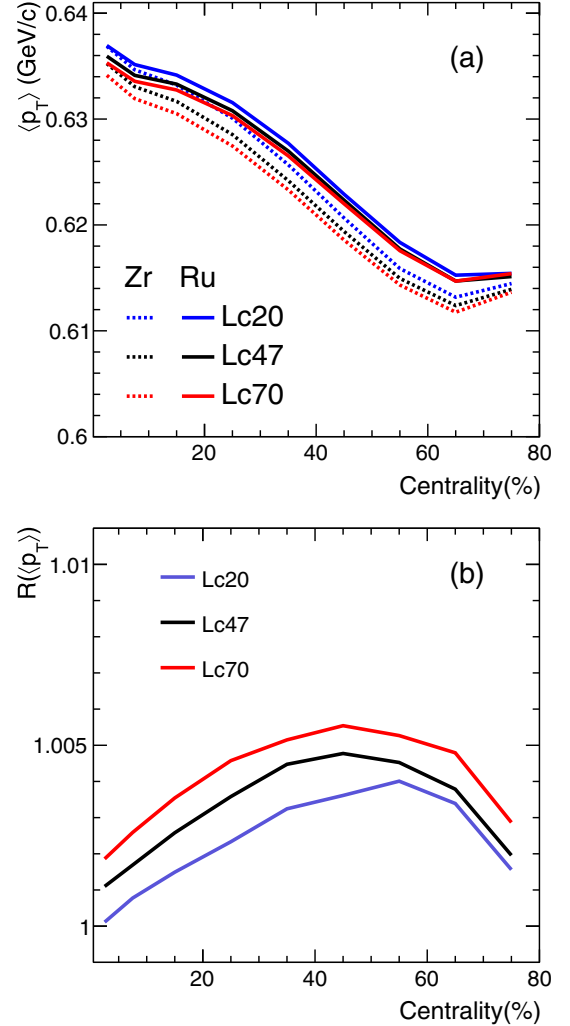

FIG. 2. (a) The mean transverse momentum $\langle p_\perp \rangle$ in $Zr + Zr$ collisions and (b) the $Ru + Ru/Zr + Zr$ ratio $R_{\langle p_\perp \rangle}$ as functions of centrality, calculated by the iEBE-VISHNU model with WS parametrization to the Lc20, Lc47, and Lc70 spherical nuclear densities.

$Ru + Ru/Zr + Zr$ ratio $R_{\langle p_\perp \rangle}$, shown in Fig. 2(b), increases with $L(\rho_c)$. This is because the neutron skin effect in ^{96}Zr is larger than that in ^{96}Ru and this effect increases with $L(\rho_c)$. The centrality dependence of $R_{\langle p_\perp \rangle}$ is nontrivial and can reach as large as 0.5% above unity.

Figure 3 shows $R_{\langle p_\perp \rangle}$ as a function of centrality for various deformation differences between Ru and Zr. The finite quadrupole deformation $\beta_2 = 0.16$ for Ru gives a significant increase in $R_{\langle p_\perp \rangle}$, and this increase is larger in noncentral collisions. This is because β_2 effectively compresses the size of the overlap area [see Eq. (5)], generating larger $\langle p_\perp \rangle$. A finite octupole deformation of $\beta_3 = 0.16$ for Zr gives a negative effect to $R_{\langle p_\perp \rangle}$ in noncentral collisions. This is because a finite β_3 can introduce an effective ϵ_2 [49]. The effect of β_3 on $R_{\langle p_\perp \rangle}$ is generally smaller than that of β_2.

Clearly, $R_{\langle p_\perp \rangle}$ depends on both the neutron skin thickness and the nuclear deformation magnitude. We present in Fig. 4 the $R_{\langle p_\perp \rangle}$ as a function of the $Ru + Ru/Zr + Zr$ ratio of $d_\perp$,
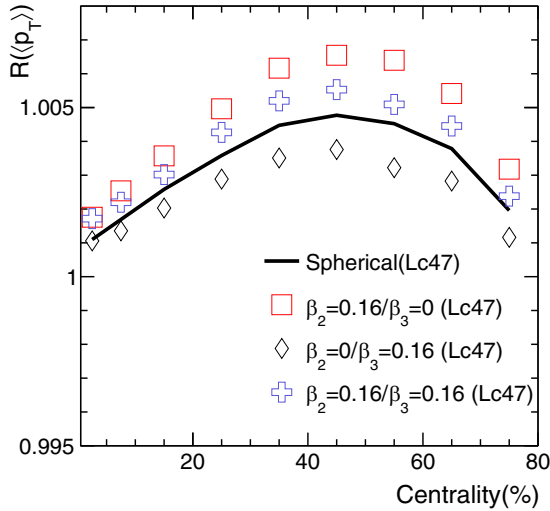
FIG. 3. The Ru + Ru/Zr + Zr ratio $R_{\langle p_\perp \rangle}$ as a function of centrality, calculated by the iEBE-VISHNU model with WS parametrization of various deformations for the ^{96}Ru and ^{96}Zr nuclei matched to the Lc47 spherical nuclear densities.

i.e., $R_{d_\perp} = d_\perp^{\mathrm{Ru+Ru}}/d_\perp^{\mathrm{Zr+Zr}}$, for the three spherical densities in solid markers and for deformed densities corresponding to the Lc47 set in open circles. The deformation effectively reduces the size of the overlap area as indicated by Eq. (5) where $r_\perp$ is matched to the spherical Lc47 density. This increases $d_\perp$, as can be seen in Fig. 4. An approximately linear relationship is observed between $R_{\langle p_\perp \rangle}$ and $R_{d_\perp}$. This confirms that $\langle p_\perp \rangle$ is primarily dependent of $d_\perp$, which is, in turn, affected by the neutron skin and the deformation of the isobar nuclei. We also show in Fig. 4 by the shaded box the effect of the factor of
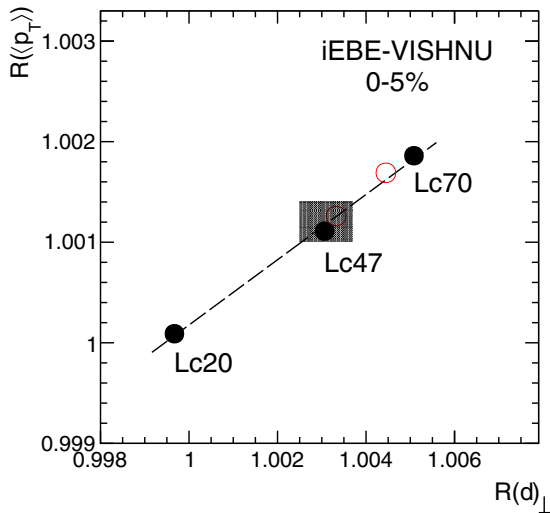

FIG. 4. The Ru + Ru/Zr + Zr ratio $R_{\langle p_\perp \rangle}$ in the top 5% centrality as a function of the transverse density ratio $R_{d_\perp}$. The solid markers show the results for WS parametrization to spherical nuclear densities (Lc20, Lc47, and Lc70); the open circles show those for deformed Ru ($\beta_2 = 0.08$ and 0.16) and spherical Zr corresponding to Lc47. The gray box indicates the uncertainties in $R_{\langle p_\perp \rangle}$ arising from a factor of 2 change in both directions in the shear and bulk viscosities.

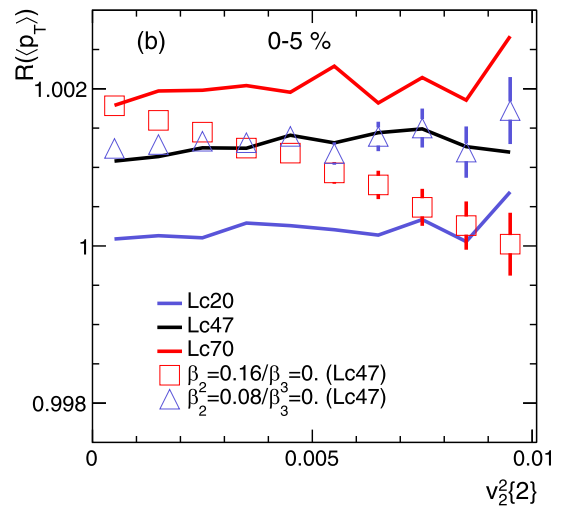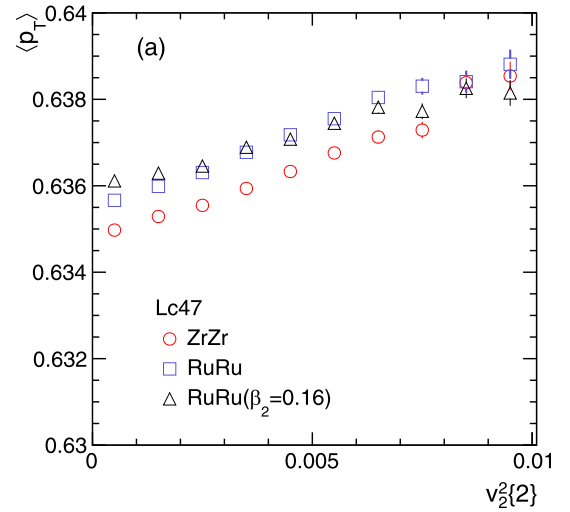

FIG. 5. (a) $\langle p_\perp \rangle$ in spherical isobar collisions and in deformed Ru + Ru collisions, and (b) the Ru + Ru/Zr + Zr ratio $R_{\langle p_\perp \rangle}$ as a function of the event-by-event $v_2^2\{2\}$ in the top 5% centrality, calculated by the iEBE-VISHNU model. The curves in panel (b) are for spherical nuclei, and the data points are for the cases of deformed Ru and spherical Zr.

2 variations in the shear and bulk viscosities in both directions; the effect is relatively small.

Both the neutron skin and deformation affect $S_\perp$; they cannot be uniquely determined by a measurement of $R_{\langle p_\perp \rangle}$. However, nuclear deformations have a large impact on anisotropic flow, particularly in central collisions [50,51]. The conversion efficiency from the initial geometry anisotropy into the final-state momentum anisotropy depends on the collision dynamics and has strong model dependence. One may avoid those model dependencies by exploiting the v_n ratios in central collisions between the two isobar systems; one complication may be nonflow contamination in v_n measurements. One may also resort to correlation measurement between $\langle p_\perp \rangle$ and the elliptic flow v_2, which has been widely discussed [14,15,52]. An anticorrelation between $\langle p_\perp \rangle$ and v_2 has been found in central collisions with deformed U + U collisions [15]. This arises from the positive correlation between $\langle r_\perp^2 \rangle$

and geometry anisotropy, e.g., a tip-tip collision gives smaller $\langle r_\perp^2 \rangle$ and ϵ_2 (and v_2). This positive correlation exceeds the anticorrelation caused by the $\sqrt{1 - \epsilon_2^2}$ term in Eq. (5). We found, however, from our hydrodynamic calculations that $\langle p_\perp \rangle$ is positively correlated with ϵ_2 in all the studied cases, even for the Ru + Ru collisions with a quadrupole deformation of $\beta_2 = 0.16$ [see Fig. 5(a)]. This is because the large fluctuations in the small isobar systems (compared to U + U) cause a significantly larger ϵ_2 in central collisions, such that $S_\perp$ is always anticorrelated with ϵ_2.

In the $\langle p_\perp \rangle$ ratio between two isobar systems, however, the effects from fluctuations are largely canceled and the difference in nuclear deformations survives. This is shown in Fig. 5(b), where $R_{\langle p_\perp \rangle}$ is calculated, within the top 5% centrality, in bins of v_2^2 which are computed by a two-particle cumulant. An anticorrelation is observed between $R_{\langle p_\perp \rangle}$ and v_2^2, the strength of which depends on the β_2 value. No such correlation is observed for the spherical nuclear densities. This anticorrelation can be used to determine the quadrupole deformation difference between ^{96}Ru and ^{96}Zr, when the deformation is relatively large. Such determination can be relatively precise as it is insensitive to the nuclear densities and may be immune to nonflow contamination in v_2. For small deformation, it may be challenging to determine its magnitude, but its effect on $R_{d\perp}$ is also small as shown in Fig. 4. Once the relative nuclear deformation is determined, the neutron skin thickness can be extracted from $R_{\langle p_\perp \rangle}$.

Conclusions. We have calculated the mean transverse momentum ratio $R_{\langle p_\perp \rangle}$ between $^{96}_{44}$Ru + $^{96}_{44}$Ru and $^{96}_{40}$Zr + $^{96}_{40}$Zr collisions with a (2+1)-dimensional viscous hydrodynamic model iEBE-VISHNU. The $R_{\langle p_\perp \rangle}$ is found to be rather insensitive to the bulk properties of the collision systems, but remains sensitive to the small differences in the nuclear structure between the ^{96}Ru and ^{96}Zr nuclei. Both the neutron skin thickness and the deformation affect the transverse overlap area $S_\perp$, which primarily determines the $\langle p_\perp \rangle$. It is found that the deformation can be determined from the correlation between $R_{\langle p_\perp \rangle}$ and the elliptic flow v_2 in central isobar collisions. The neutron skin thickness can in turn be determined from $R_{\langle p_\perp \rangle}$, which would complement low-energy nuclear interaction experiments to probe the symmetry energy density slope parameter.

[1] J. Adams *et al.* (STAR Collaboration), Nucl. Phys. A **757**, 102 (2005).

[2] K. Adcox *et al.* (PHENIX Collaboration), Nucl. Phys. A **757**, 184 (2005).

[3] K. Aamodt *et al.* (ALICE Collaboration), Phys. Rev. Lett. **105**, 252302 (2010).

[4] M. Gyulassy, I. Vitev, X.-N. Wang, and B.-W. Zhang, in *Quark-Gluon Plasma 3*, edited by R. C. Hwa and X. N. Wang (World Scientific, Singapore, 2004), pp. 123–191.

[5] C. Gale, S. Jeon, and B. Schenke, Int. J. Mod. Phys. A **28**, 1340011 (2013).

[6] P. K. Kovtun, D. T. Son, and A. O. Starinets, Phys. Rev. Lett. **94**, 111601 (2005).

[7] P. Romatschke and U. Romatschke, Phys. Rev. Lett. **99**, 172301 (2007).

[8] H. Song, S. A. Bass, U. Heinz, T. Hirano, and C. Shen, Phys. Rev. Lett. **106**, 192301 (2011); **109**, 139904(E) (2012).

[9] H.-j. Xu, Z. Li, and H. Song, Phys. Rev. C **93**, 064905 (2016).

[10] W. Zhao, H.-j. Xu, and H. Song, Eur. Phys. J. C **77**, 645 (2017).

[11] W. Broniowski, M. Chojnacki, and L. Obara, Phys. Rev. C **80**, 051902(R) (2009).

[12] P. Bozek and W. Broniowski, Phys. Rev. C **85**, 044910 (2012).

[13] A. Mazeliauskas and D. Teaney, Phys. Rev. C **93**, 024913 (2016).

[14] B. Schenke, C. Shen, and D. Teaney, Phys. Rev. C **102**, 034905 (2020).

[15] G. Giacalone, F. G. Gardim, J. Noronha-Hostler, and J.-Y. Ollitrault, Phys. Rev. C **103**, 024909 (2021).

[16] G. Giacalone, Phys. Rev. Lett. **124**, 202301 (2020).

[17] J. Jia, Phys. Rev. C **105**, 044905 (2022).

[18] S. Ryu, J. F. Paquet, C. Shen, G. S. Denicol, B. Schenke, S. Jeon, and C. Gale, Phys. Rev. Lett. **115**, 132301 (2015).

[19] J. E. Bernhard, J. S. Moreland, and S. A. Bass, Nat. Phys. **15**, 1113 (2019).

[20] D. E. Kharzeev, L. D. McLerran, and H. J. Warringa, Nucl. Phys. A **803**, 227 (2008).

[21] S. A. Voloshin, Phys. Rev. Lett. **105**, 172301 (2010).

[22] D. E. Kharzeev, J. Liao, S. A. Voloshin, and G. Wang, Prog. Part. Nucl. Phys. **88**, 1 (2016).

[23] W.-T. Deng, X.-G. Huang, G.-L. Ma, and G. Wang, Phys. Rev. C **94**, 041901(R) (2016).

[24] J. Zhao and F. Wang, Prog. Part. Nucl. Phys. **107**, 200 (2019).

[25] J. Adam *et al.* (STAR Collaboration), Nucl. Sci. Tech. **32**, 48 (2021).

[26] M. Abdallah *et al.* (STAR Collaboration), Phys. Rev. C **105**, 014901 (2022).

[27] H.-J. Xu, X. Wang, H. Li, J. Zhao, Z.-W. Lin, C. Shen, and F. Wang, Phys. Rev. Lett. **121**, 022301 (2018).

[28] H. Li, H.-j. Xu, J. Zhao, Z.-W. Lin, H. Zhang, X. Wang, C. Shen, and F. Wang, Phys. Rev. C **98**, 054907 (2018).

[29] H.-j. Xu, H. Li, X. Wang, C. Shen, and F. Wang, Phys. Lett. B **819**, 136453 (2021).

[30] H. Li, H.-j. Xu, Y. Zhou, X. Wang, J. Zhao, L.-W. Chen, and F. Wang, Phys. Rev. Lett. **125**, 222301 (2020).

[31] L.-W. Chen, C. M. Ko, and B.-A. Li, Phys. Rev. C **72**, 064309 (2005).

[32] X. Roca-Maza, M. Centelles, X. Vinas, and M. Warda, Phys. Rev. Lett. **106**, 252501 (2011).

[33] M. B. Tsang *et al.*, Phys. Rev. C **86**, 015803 (2012).

[34] A. Tamii *et al.*, Phys. Rev. Lett. **107**, 062502 (2011).

[35] Z. Zhang and L.-W. Chen, Phys. Rev. C **90**, 064317 (2014).

[36] Z. Zhang and L.-W. Chen, Phys. Lett. B **726**, 234 (2013).

[37] Y. Zhou, L.-W. Chen, and Z. Zhang, Phys. Rev. D **99**, 121301(R) (2019).

[38] D. Adhikari *et al.* (PREX Collaboration), Phys. Rev. Lett. **126**, 172502 (2021).

[39] B. T. Reed, F. J. Fattoyev, C. J. Horowitz, and J. Piekarewicz, Phys. Rev. Lett. **126**, 172503 (2021).

[40] H. Song and U. W. Heinz, Phys. Rev. C **77**, 064901 (2008).

[41] C. Shen, Z. Qiu, H. Song, J. Bernhard, S. Bass, and U. Heinz, Comput. Phys. Commun. **199**, 61 (2016).

[42] J. E. Bernhard, J. S. Moreland, S. A. Bass, J. Liu, and U. Heinz, Phys. Rev. C **94**, 024907 (2016).

[43] S. A. Bass *et al.*, Prog. Part. Nucl. Phys. **41**, 255 (1998).

[44] M. Bleicher *et al.*, J. Phys. G: Nucl. Part. Phys. **25**, 1859 (1999).

[45] J. S. Moreland, J. E. Bernhard, and S. A. Bass, Phys. Rev. C **92**, 011901(R) (2015).

[46] H.-j. Xu, H. Li, Y. Zhou, X. Wang, J. Zhao, L.-W. Chen, and F. Wang, Phys. Rev. C **105**, L011901 (2022).

[47] C. Zhang and J. Jia, Phys. Rev. Lett. **128**, 022301 (2022).

[48] R. S. Bhalerao, J.-P. Blaizot, N. Borghini, and J.-Y. Ollitrault, Phys. Lett. B **627**, 49 (2005).

[49] J. Jia, Phys. Rev. C **105**, 014905 (2022).

[50] U. W. Heinz and A. Kuhlman, Phys. Rev. Lett. **94**, 132301 (2005).

[51] P. Filip, R. Lednicky, H. Masui, and N. Xu, Phys. Rev. C **80**, 054903 (2009).

[52] G. Giacalone, Phys. Rev. C **102**, 024901 (2020).